Modelling and prevention of acute kidney injury through ischemia and reperfusion in a combined human renal proximal Tubule/Blood Vessel-on-a-Chip

Tool, L.; Vormann, M.; Ohbuchi, M.; Gijzen, L.; Vught, R. van; Hankemeier, T.; ... ; Tetsuka, K.

Kidney360

Modelling and Prevention of Acute Kidney Injury through Ischemia and Reperfusion in a Combined Human Renal Proximal Tubule/Blood Vessel-on-a-Chip

Marianne K. Vormann,[1] Laura M. Tool,[1] Masato Ohbuchi,[2] Linda Gijzen,[1] Remko van Vught,[1] Thomas Hankemeier,[3] Fumiko Kiyonaga,[4] Tetsuhiro Kawabe,[5] Takayuki Goto,[5] Akira Fujimori,[6] Paul Vulto,[1] Henriette L. Lanz,[1] and Kazuhiro Tetsuka[2]

Key Points

- We set up an *in vitro* proximal tubule model that can capture acute kidney damage after an ischemic event.
- We showed the renoprotective effect of adenosine in an *in vitro* AKI/rIRI on-a-chip model.
- We showed a robust model for AKI/rIRI that can be used for high-throughput testing.

Abstract

Background Renal ischemia/reperfusion injury (rIRI) is one of the major causes of AKI. Although animal models are suitable for investigating systemic symptoms of AKI, they are limited in translatability. Human *in vitro* models are crucial in giving mechanistic insights into rIRI; however, they miss out on crucial aspects such as reperfusion injury and the multitissue aspect of AKI.

Methods We advanced the current renal proximal tubule-on-a-chip model to a coculture model with a perfused endothelial vessel separated by an extracellular matrix. The coculture was characterized for its three-dimensional structure, protein expression, and response to nephrotoxins. Then, rIRI was captured through control of oxygen levels, nutrient availability, and perfusion flow settings. Injury was quantified through morphologic assessment, caspase-3/7 activation, and cell viability.

Results The combination of low oxygen, reduced glucose, and interrupted flow was potent to disturb the proximal tubules. This effect was strongly amplified upon reperfusion. Endothelial vessels were less sensitive to the ischemia–reperfusion parameters. Adenosine treatment showed a protective effect on the disruption of the epithelium and on the caspase-3/7 activation.

Conclusions A human *in vitro* rIRI model was developed using a coculture of a proximal tubule and blood vessel on-a-chip, which was used to characterize the renoprotective effect of adenosine. The robustness of the model and assays in combination with the throughput of the platform make it ideal to advance pathophysiological research and enable the development of novel therapeutic modalities.

KIDNEY360 3: 217–231, 2022. doi: https://doi.org/10.34067/KID.0003622021

Introduction

AKI is a severe medical problem with a high mortality rate. Every year, around 1.7 million people die of AKI worldwide (1,2). Because the kidney is responsible for eliminating waste products from the blood, it encounters high concentrations of xenobiotics and is therefore vulnerable for (drug-induced) toxicity (3,4). In the kidney, renal proximal tubule epithelial cells (RPTEC) express many ATP-dependent transporters and play important roles in reabsorption of essential nutrients. RPTEC have a high energy demand to drive active transporters, and renal blood flow supplies the required oxygen (5,6). Patients with a disrupted renal flow because of either prerenal hypoperfusion (*e.g.*, heart failure or hemorrhage) or postrenal obstruction (*e.g.*, cancer or a blood clot) also suffer from AKI (3,7). Renal ischemia/reperfusion injury (rIRI) causes a loss of function and cell damage of the proximal tubule structure, ultimately leading to AKI (8–10). Recently, AKI has been extensively researched as a symptom after severe acute respiratory syndrome coronavirus 2 infection (11).

[1]Mimetas BV, Oegstgeest, The Netherlands
[2]Analysis and Pharmacokinetics Research Labs, Astellas Pharma, Inc., Ibaraki, Japan
[3]LACDR, Leiden University, The Netherlands
[4]Innovation and Incubation Research Labs, Astellas Pharma, Inc., Ibaraki, Japan
[5]Modality Research Labs, Astellas Pharma, Inc., Ibaraki, Japan
[6]Research Portfolio Planning, Astellas Pharma, Inc., Ibaraki, Japan

Correspondence: Henriette L. Lanz, De Limes 7, 2342 DH, Oegstgeest, The Netherlands, or Kazuhiro Tetsuka, 21 Miyukigaoka, Tsukuba-shi Ibaraki, 305-8585, Japan. Email: h.lanz@mimetas.com or Kazuhiro.Tetsuka@astellas.com

For investigating the pathophysiology of rIRI and drug screening for AKI, animal models are widely used to capture the systemic symptoms of AKI (12). However, here, a significant species difference between animal and human is observed (13). Not all drug candidates that showed efficacy in animal models showed efficacy in AKI treatment in clinical trials. *In vitro* cellular models are also applied for elucidation of rIRI/AKI mechanistic insights (14). Unfortunately, traditional two-dimensional culture settings of RPTEC lack their typical structure and their associated functionality (15,16). *In vitro* experiments do provide a controlled environment, allowing manipulation of specific variables such as flow and incubated oxygen levels, and enabling higher reproducibility (14). Finally, the replacement of animal models is expected to reduce costs and time and increase the throughput and predictability (17,18).

Human cellular models can be valuable tools for tackling rIRI and discovering AKI preventive agents (19). *In vitro* rIRI models have been reported that enable induction of hypoxia by chemical induction, enzymatic induction, or anaerobic chambers (14). However, additional parameters are important to mimic ischemia-inducing insults comprehensively (20). Loss of nutrients, loss of flow, and the buildup of waste products, and the reset of all parameters upon reperfusion can cause damage and should be included in rIRI modeling. Recent advances in tissue engineering and microfluidic cell culture techniques have made significant progress in modeling key aspects of human organs *in vitro* (15). Different microfluidic chip setups have been used to model the proximal tubule, which offer physiologic realism in cell and tissue function to study, for example, nephrotoxicity and drug-drug interaction (reviewed by Vedula and Charest [21]). Application of shear stress to the apical side is important because it regulates tight-junction and polarized transporter localization, and the inclusion of a basement membrane (22–25). We have previously reported a human proximal tubule on-a-chip model composed of 40 perfused proximal tubules grown against an extracellular matrix (ECM) (26). We showed the utility of this model for assessing kidney toxicity, drug-drug interaction, and transporter function (26–28).

In this study, we developed an advanced model to study rIRI comprising a perfused three-dimensional (3D) proximal tubule adjacent to a 3D perfused blood vessel. The proximal tubule and blood vessel are separated by a type 1 collagen surrogate ECM. We characterized the culture using immunostaining for cell type specific markers and ensured correct polarization. We then validated the response to nephrotoxicants. We modeled rIRI by adjusting culture parameters such as incubated oxygen concentration, perfusion flow, and nutrients such as glucose, followed by a return to normal culture conditions. Finally, we assessed the protective potential of adenosine, nicotinamide, and N-acetylcysteine (NAC) that have been reported to prevent rIRI in animal models (29–33). With 40 chips on one standard multiwell plate, the model is compatible with screening. We foresee that this new human rIRI model will provide a springboard for the development of preventative or curative treatments for ischemic AKI.

Materials and Methods

Cell Culture

Human RPTEC (Kidney PTEC Control Cells, SA7K Clone, MTOX1030; Sigma–Aldrich) were cultured on PureCol-coated (Advanced BioMetrix, 5005-B, diluted with 1:30 in HBSS [H6648; Sigma–Aldrich], 20 minutes of incubation at 37°C) T75 flasks (431464U; Corning) in MEME alpha Modification (M4526; Sigma–Aldrich) supplemented with RPTEC Complete Supplement (MTOXRCSUP; Sigma–Aldrich), L-glutamine (1.87 mM, G7513; Sigma–Aldrich), gentamicin (28 μg/ml, G1397; Sigma–Aldrich), and amphotericin B (14 ng/ml, A2942; Sigma–Aldrich). Cells were incubated in a humidified incubator (37°C, 5% CO_2), and medium was changed every 2–3 days. At 90%–100% confluency, cells were washed with HBSS, detached with Accutase (A6964; Sigma–Aldrich), neutralized with culture medium, pelleted (140 *g*, 5 minutes), and used for seeding in the OrganoPlate. Cells were used up to passage 3.

Human umbilical vein endothelial cells (HUVEC; C2519A; Lonza) were cultured on surface-treated T75 (156499; Thermo Fisher Scientific) flasks in MV2 complete medium (Endothelial Cell Medium MV2, C-22022; Promocell) supplemented with Supplement Mix Endothelial Cell Growth Medium MV2 (C-39226; Promocell), and 1% pen/strep (P4333; Sigma–Aldrich). Cells were incubated in a humidified incubator (37°C, 5% CO_2), and medium was changed every 2–3 days. At 90%–100% confluency, cells were washed with HEPES-BSS (CC-5022; Lonza), detached with 0.025% Trypsin-EDTA (1×) solution (CC-5012; Lonza), neutralized with Trypsin Neutralizing Solution (CC-5002; Lonza), pelleted (200 *g*, 5 minutes), and used for seeding in the OrganoPlate. Cells were used up to passage 9.

Establishment of the RPTEC-HUVEC Coculture

For all experiments, the OrganoPlate 3-lane (4003 400B; Mimetas BV) was used. Figure 1A shows a photograph of the bottom of the OrganoPlate, demonstrating the 40 microfluidic channel networks, glued to a standard 384-well plate. A zoom-in on a single chip highlights the region of interest where three microfluidic channels join in the center (Figure 1B, green circle). The three channels are separated by phaseguides, which are small ridges that prevent overflow between adjacent channels through meniscus pinning (34) (Figure 1C, gray bars).

As a starting point for the seeding, we took the RPTEC monoculture protocol, as previously described (26), and introduced a seeding procedure for an endothelial vessel alongside the RPTEC tubule (Figure 1, D–F). In short, 2 μl of a liquefied ECM gel composed of 4 mg/ml type 1 collagen was loaded into the middle inlet of all 40 chips and allowed to polymerize (Figure 1D, step 1). The following day, RPTECs were seeded against the gel to the top channel and allowed to adhere (Figure 1D, step 2). After attachment of the cells, medium was added, and the OrganoPlate was placed in an incubator on an interval rocker platform (MI-OFPR-L; Mimetas BV; ±7° angle, 8-minute interval), enabling a passive, bidirectional flow through the perfusion channels (Figure 1D, step 3).

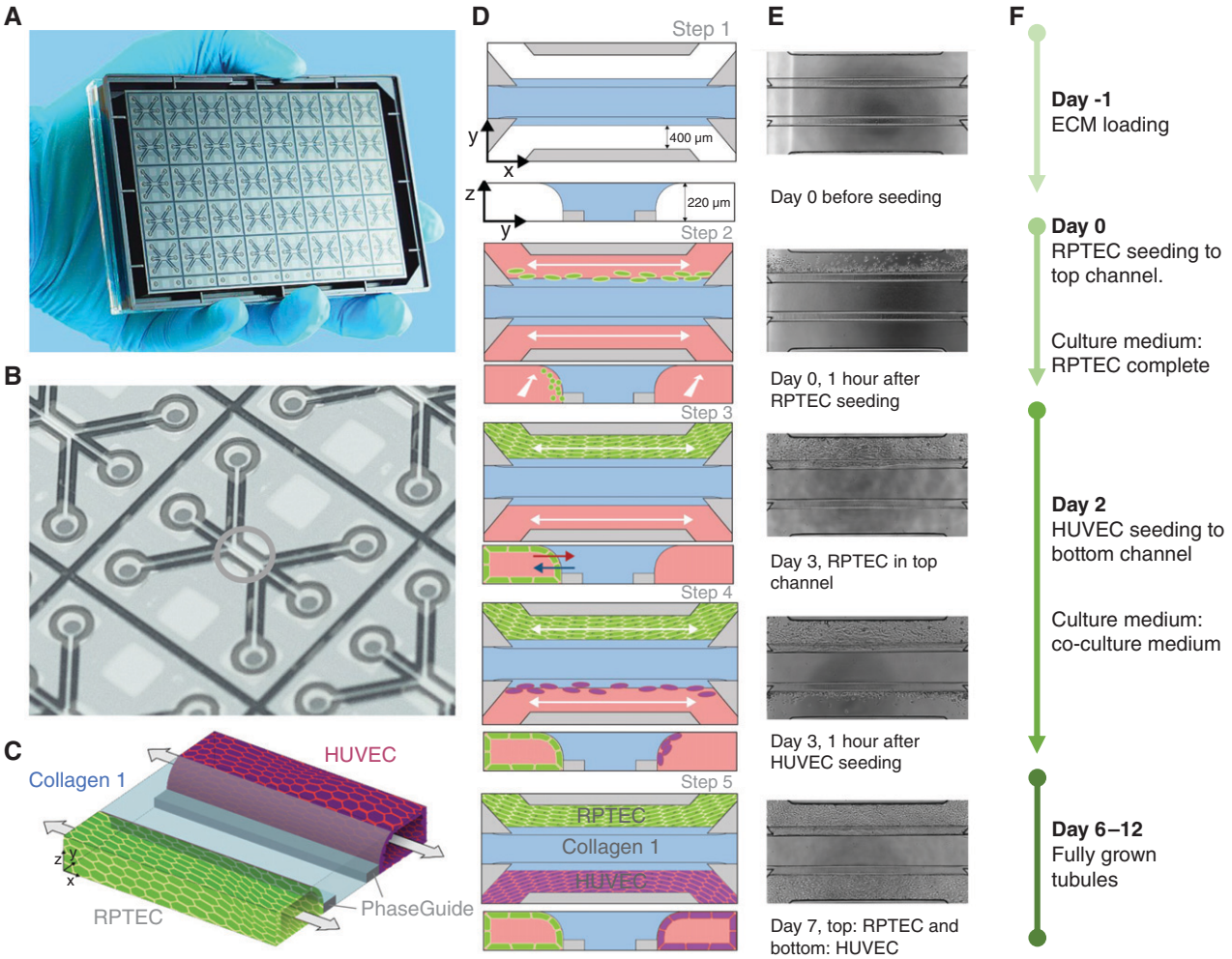

Figure 1. | Overview of the seeding method of the renal proximal tubule epithelial cells (RPTEC)/human umbilical vein endothelial cells (HUVEC) coculture in the OrganoPlate 3-lane. (A) Photograph of the bottom of the culture platform showing 40 microfluidic channel networks underneath a 384-well plate. (B) Zoom-in on a single microfluidic channel network comprising three channels that join in the center (green circle). (C) Three-dimensional artist impression of the center of a chip, where two tubules are cultured in the two lateral channels (green and purple) along an extracellular matrix (ECM) gel in the middle channel (light blue). Two phaseguides (gray bars) define the positioning of the ECM gel leading to the three-lane stratified profile. (D) Artist impression of the horizontal projection and vertical cross-section. (E) Associated phase-contrast images. (F) Timeline for setting up the coculture.

HUVEC were added to the bottom channel of the microfluidic chip on day 2 (Figure 1D, step 4). HUVEC were detached as described above and re-suspended in MV2 complete medium at a concentration of 10×10^6 cells/ml. Medium from all bottom in- and outlets was aspirated, and the plate was turned 180°, resulting in RPTEC tubes sitting in the bottom. Two microliters of the HUVEC cell suspension was added to the (new) top-left inlet. Subsequently, 1 µl was aspirated *via* the outlet from the top channel to guide HUVEC through the system. The OrganoPlate was placed on its side at an angle of 75° to allow the HUVEC attach to the ECM. After an incubation time of 60 minutes, medium from both channels was switched to coculture medium (50% CellBiologics complete human endothelial cell medium (basal medium with the growth factor supplement kit [H1168]) and 50% RPTEC complete medium). Perfusion was applied again, resulting in fully grown tubules of RPTEC and HUVEC on day 6 (Figure 1, C and D, step 5). Cocultures were used for experiments up to day 12. The timeline of coculture seeding was determined in an optimization study (data not shown), with RPTEC seeded on day 0 and HUVEC on day 2 (Figure 1, D–F).

Immunohistochemistry

Cocultures were fixed by replacing the medium with 4% formaldehyde (252549; Sigma–Aldrich) in HBSS (55037C; Sigma–Aldrich) for 10 minutes. Tubules were washed with washing solution (4% FBS [16140–071; Gibco] in HBSS) and permeabilized (0.3% Triton X-100 [T8787; Sigma–Aldrich] in HBSS) for 10 minutes. Next, cultures were incubated for 45 minutes in blocking solution (2% FBS, 2% BSA [A2153; Sigma–Aldrich], and 0.1% Tween 20 [P9416; Sigma–Aldrich] in HBSS). Hereafter, cultures were incubated with the primary antibodies and diluted in blocking solution for 60 minutes at room temperature. Primary antibodies

Table 1. Nephrotoxic compounds used for validation of the model

Compound	Catalog Number (Sigma–Aldrich)	Solvent	Final Vehicle Concentration, v/v, (%)	Highest Concentration
Cisplatin	P4394	0.9% NaCl in H2O	5.4	270 μM
Tobramycin	T1783	Culture medium	—	50 mM
Cyclosporin A	30024	DMSO	0.6	60 μM
Staurosporine	S4400	DMSO	0.1	10 μM
Dexamethasone	D4902	DMSO	0.1	30 μM

against Ms-a-ezrin (610602; BD Biosciences; 1:200), Ms-a-acetylated tubulin (T6793; Sigma–Aldrich; 1:4000), Rb-a-Zonula occludens-1 (ZO-1; 61–7300; Thermo Fisher Scientific; 1:125), and Rb-a-VE-cadherin (Ab33168; Abcam; 1:1000) were used. Subsequently, cultures were washed twice with washing solution for 5 minutes each and then incubated for 30 minutes at room temperature with secondary antibodies Gt-a-Ms IgG (H+L) Alexa Fluor 555 (A21422; Thermo Fisher Scientific; 1:250) and Gt-a-Rb IgG (H+L) Alexa Fluor 488 (A32731; Thermo Fisher Scientific; 1:250) diluted in blocking solution. After washing the tubules twice for 5 minutes, nuclei were stained with Hoechst 33342 (H3570; Thermo Fisher Scientific; 1:2000) in the last washing step. Fluorescent images for the 3D reconstructions were taken with the ImageXpress Micro Confocal High-Content Imaging System (Molecular Devices). A z-stack of 220 μm with 2 μm between each image plane was acquired for DAPI, FITC, and TRITC channels. Three-dimensional reconstructions and maximum projections were created using ImageJ (35).

Nephrotoxicant Exposure

Cultures were exposed to a concentration range of cisplatin, tobramycin, and cyclosporin A (CysA) (36) (Table 1). Staurosporine (10 μM), a well-known apoptosis inducer (37), was included as a positive control, and dexamethasone (30 μM) (38) as a negative control. On day 6, medium of both channels was replaced with coculture medium complemented with a nephrotoxicant, the positive or the negative control (Table 1). After a 48-hour incubation on the rocker platform, medium was sampled from the top wells connected to the RPTEC tubules. Samples from the in- and outlet were pooled and used for the lactate dehydrogenase (LDH) activity assay. Tubules were thereafter incubated with WST-8 buffer diluted in medium to determine viability. Phase-contrast and fluorescent images were acquired using the ImageXpress XLS Micro Confocal High-Content Imaging System to assess the morphology of the cells and their nuclei. Moreover, activation of caspase-3/7 activity was visualized.

Fluorogenic Caspase-3/7 Assay and Nuclei Staining

For acquiring live cell images of cells undergoing caspase-3/7-mediated apoptosis, culture medium was replaced with medium containing caspase-3/7 green apoptosis assay reagent (dilution 1:1000; #4440; Sartorius). After a 1.5-hour incubation at 37°C, 21% O_2, 5% CO_2 on the rocker platform, a z-stack of 220 μm with 5 μm between each image plane was acquired for FITC using the ImageXpress Micro Confocal High-Content Imaging System with a ×10 objective. The plate was thereafter fixated as described previously (26), and nuclei were stained with Hoechst 33342 and imaged again for DAPI. One maximum projection per chip was created for both DAPI and FITC using ImageJ.

LDH Activity Assay

LDH activity of the samples was determined using the Lactate Dehydrogenase Activity Assay Kit (MAK066; Sigma–Aldrich) according to the manufacturer's protocol. In short, the medium of the top in- and outlet or bottom in- and outlet was pooled for RPTEC or HUVEC, respectively. Two microliters was added in duplicate to a black 384-well plate with a glass bottom. Next, 18-μl LDH assay buffer was added to all sample wells to make an initial volume of 20 μl. In parallel, a concentration curve of the NADH standard was added. After a short centrifugation step, 20-μl Master Reaction Mix was added to each well. After 1 minute, the absorbance was measured with the Multiskan FC Microplate Photometer (Thermo Fisher Scientific) at 450 nm every 2 minutes for 6 minutes. Background subtraction was performed using the results of cell-free chips exposed to medium without any additives. The LDH activity was determined using the following formula:

$$\text{LDH activity (nmol/min per ml)} = \frac{\text{nmol NADH} \times \text{sample dilution factor}}{\text{reaction time (min)} \times \text{sample volume (ml)}}$$

Cell Viability (WST-8 assay)

The viability of the cells was determined using the Cell Counting Kit-8 (96992; Sigma–Aldrich). The WST-8 solution was diluted 1:11 with coculture medium and added to both perfusion channels of one chip (30 μl in- and outlets). After an 18-minute incubation at 37°C and 5% CO_2 on the rocker platform and a 2-minute static incubation, the absorbance in the top in- and outlets was measured with the MultiskanFC Microplate Photometer (Thermo Fisher Scientific) at 450 nm. For background subtraction, measurements from cell-free chips were used.

Modeling Renal Ischemia and Renal Reperfusion

Renal ischemia was modeled on the OrganoPlate cocultures by exposing the cultures to low oxygen (5% O_2) and/or low glucose and nutrient availability and/or no perfusion. This was compared with a normoxic culture: atmospheric O_2 of 21%, coculture medium, and perfusion. Eight different setups were tested (Table 2).

Table 2. Conditions used to model ischemia

Condition (Abbreviation)	Incubator-Oxygen Tension	Perfusion	Glucose and Nutrient Availability
N+P+glu	Normoxia (21% O_2)	Yes (rocker)	Coculture medium
N+P-glu	Normoxia (21% O_2)	Yes (rocker)	DMEM w/o glucose
N+S+glu	Normoxia (21% O_2)	No (static)	Coculture medium
N+S-glu	Normoxia (21% O_2)	No (static)	DMEM w/o glucose
L+P+glu	Low oxygen (5% O_2)	Yes (rocker)	Coculture medium
L+P-glu	Low oxygen (5% O_2)	Yes (rocker)	DMEM w/o glucose
L+S+glu	Low oxygen (5% O_2)	No (static)	Coculture medium
L+S-glu	Low oxygen (5% O_2)	No (static)	DMEM w/o glucose

N, normoxia; L, low oxygen; P, perfusion; S, static; +glu, coculture medium; -glu, DMEM w/o glucose.

Table 3. Protective compounds tested to prevent cell damage during renal ischemia and reperfusion

Compound	Supplier, Catalog Number	Solvent	Stock Concentration, mM	Exposure Concentration, mM
Adenosine	Sigma–Aldrich, A4036	1M NH4OH (heated) Sigma–Aldrich, 09859	180	1
Nicotinamide	Sigma–Aldrich, N0636	Milli-Q	1000	10
N-acetylcysteine	Sigma–Aldrich, A9165	Milli-Q	500	1

On day 6 of the coculture, ischemic conditions were induced. For lowering expected oxygen levels, cultures were placed in a low oxygen incubator (5% CO_2, 37°C, 5% O_2). Perfusion was stopped by removing the plates from the rocker platform. For low nutrient cultures, the medium was changed to DMEM without glucose (#11966025; Gibco). The cultures were exposed to combinations of the ischemic conditions for 24 hours, after which medium was sampled for the LDH assay and phase-contrast images were acquired. To model rIRI, the exposure was followed by a reperfusion of the cultures for another 24 hours in normoxic conditions. Subsequently, medium was sampled for LDH assay, WST-8 viability was determined, phase-contrast images were acquired, and the cultures were stained for DNA and caspase-3/7 activation.

Assessment of Potential Protective Compounds

Prevention of ischemic damage during exposure and reperfusion of the cultures was assessed upon addition of adenosine, nicotinamide, and NAC during exposure and reperfusion to the culture medium of both channels (Table 3). For testing possible protecting effects of the coincubation with the three compounds, cultures were exposed to the selected ischemic conditions L+P-glu and L+S-glu and compared with the N+P+glu control. The experiment was executed with an ischemia exposure time of 12 or 24 hours, both followed by 24-hour reperfusion. LDH activity samples and phase-contrast images were acquired after the exposure and after reperfusion. WST-8 viability assay and DNA and caspase-3/7 staining were performed after reperfusion only. Staurosporine (10 μM) was used as positive control for the viability assays.

Real-Time Imaging

On day 6 of culture, the plate was placed in the EVOS FL Auto Imaging System (Life Technologies, 5% CO_2, 37°C, humidified) and incubated static in DMEM without glucose medium under 5% O_2 (L+S-glu) for 24 hours to mimic an ischemic event. Phase-contrast and FITC images were acquired every 32 minutes for 24 hours. Hereafter, the plate was reperfused with nutrient-rich coculture medium in normoxia (21% O_2), and perfusion was reinstated by placing the EVOS FL Auto Imaging System on a rocker platform (7° angle, 8-minute interval) for another 24 hours, while phase-contrast and FITC images were acquired every 32 minutes. During the exposure and reperfusion, cultures were coincubated with or without 1-mM adenosine. To monitor the activation of caspase-3/7, the caspase-3/7 green apoptosis assay reagent was added to the medium (1:1000).

Data Analysis and Statistics

Images were processed using ImageJ (35). Data points with technical errors (such as failure of ECM filling, inadequate cell growth, or air bubble trapping by microscopic observation) were excluded before analysis. Data analysis was performed using Excel (Microsoft Office 365 Business) and GraphPad Prism (GraphPad Software, Inc., version 8.4.2). Error bars represent the standard deviation. One-way ANOVA was used for statistical analysis between groups followed by Tukey's multiple comparisons test. A log(y) transformation was used to normalize the data if indicated by Anderson–Darling test or Brown Forsythe test of variances. In case of negative values, data were transformed using log(y+1). A P value of <0.05 was considered as significant.

Results

Perfused Coculture of Epithelial Tubules and Endothelial Vessels Was Established in a Microfluidic Chip

Figure 1 illustrates the setup for the perfused coculture of a human renal proximal tubule-on-a-chip and a blood

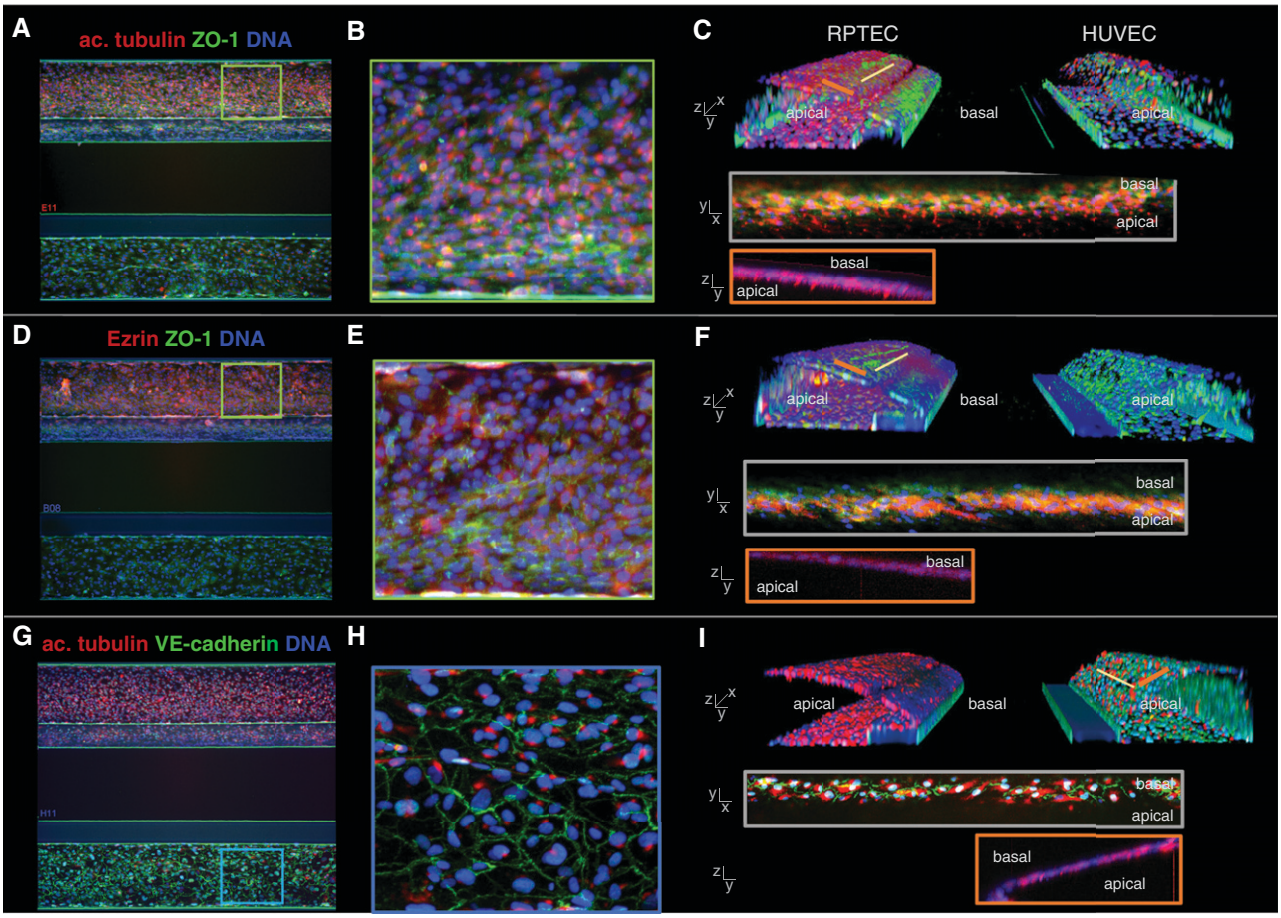

Figure 2. | **Marker expression of the kidney model shows polarized epithelium and endothelium.** (A, D, and G) Max z-projections of the coculture with the RPTEC tubule in the top channel and the HUVEC vessel in the bottom channel. (B, E, and H) Zoom of the z-projections in (A), (D), and (G). (C, F, and I) three-dimensional reconstructions showing a view into the lumen of the tubules. (A–C) Primary cilia were visualized by acetylated tubulin staining (red), present on the apical side of the RPTEC tubule. Tight junction protein ZO-1 (green) was present in both cell types. (D–F) Epithelial marker and brush border protein Ezrin (red) was exclusively present on the apical side of the RPTEC tubule. (G–I) Endothelial tight junction protein VE-cadherin (green) was expressed by the HUVEC vessel at the cell border, and primary cilia located on the apical side of the membrane were stained using acetylated tubulin.

vessel. RPTEC are cultured in the OrganoPlate 3-lane system against a type 1 collagen ECM mimic and formed a tubular structure upon application of perfusion flow. At the same time, a blood vessel was grown from HUVECs against the ECM on the other side. The three-lane stratified setup is achieved by patterning a type 1 collagen gel in the center of the chip using capillary pinning barriers called phaseguides (34).

Figure 2 shows immunohistochemical staining's of the coculture model from a top view (Figure 2, A, B, D, E, G, and H) and a 3D bird's-eye view (Figure 2, C, F, and I). Tight junctions were confirmed through ZO-1 expression (Figure 2, A–F, green) (39). Acetylated tubulin staining showed one primary cilium per cell on the luminal side for both cell types (Figure 2, A–C and G–I, red) (40,41). Epithelial marker and brush border protein Ezrin (42) was exclusively located on the apical side of the RPTEC layer (Figure 2, D–F, red). Endothelial adherence junction protein VE-cadherin (43) was expressed by the endothelial cells at the cell borders (Figure 2, G–I, green).

A 3D reconstruction of the coculture obtained by confocal microscopy showed that RPTEC and HUVEC adhered to the ECM in the central channel and grew to confluency after 6 and 4 days, respectively (Figure 2, C, F, and I). A view on the cross-section of both structures showed lumen formation on both sides of ECM, with the basal sides of the membranes facing each other.

Perfused 3D Renal Proximal Tubule and Blood Vessel-on-a-Chip Is Sensitive to Nephrotoxicants

Next, we assessed the response of the model to cisplatin, tobramycin, and CysA after 48 hours of exposure. Phase-contrast imaging showed rounded-up and clustered cells for high concentrations of cisplatin and tobramycin, whereas the morphology of the culture upon CysA exposure remained normal for all concentrations (Figure 3A).

DNA staining (Figure 3B) and activated caspase-3/7 staining (44) (Figure 3C) confirmed these observations, showing visible damage for concentration of 27-μM cisplatin or 28.1-mM tobramycin and higher. Tubules exposed

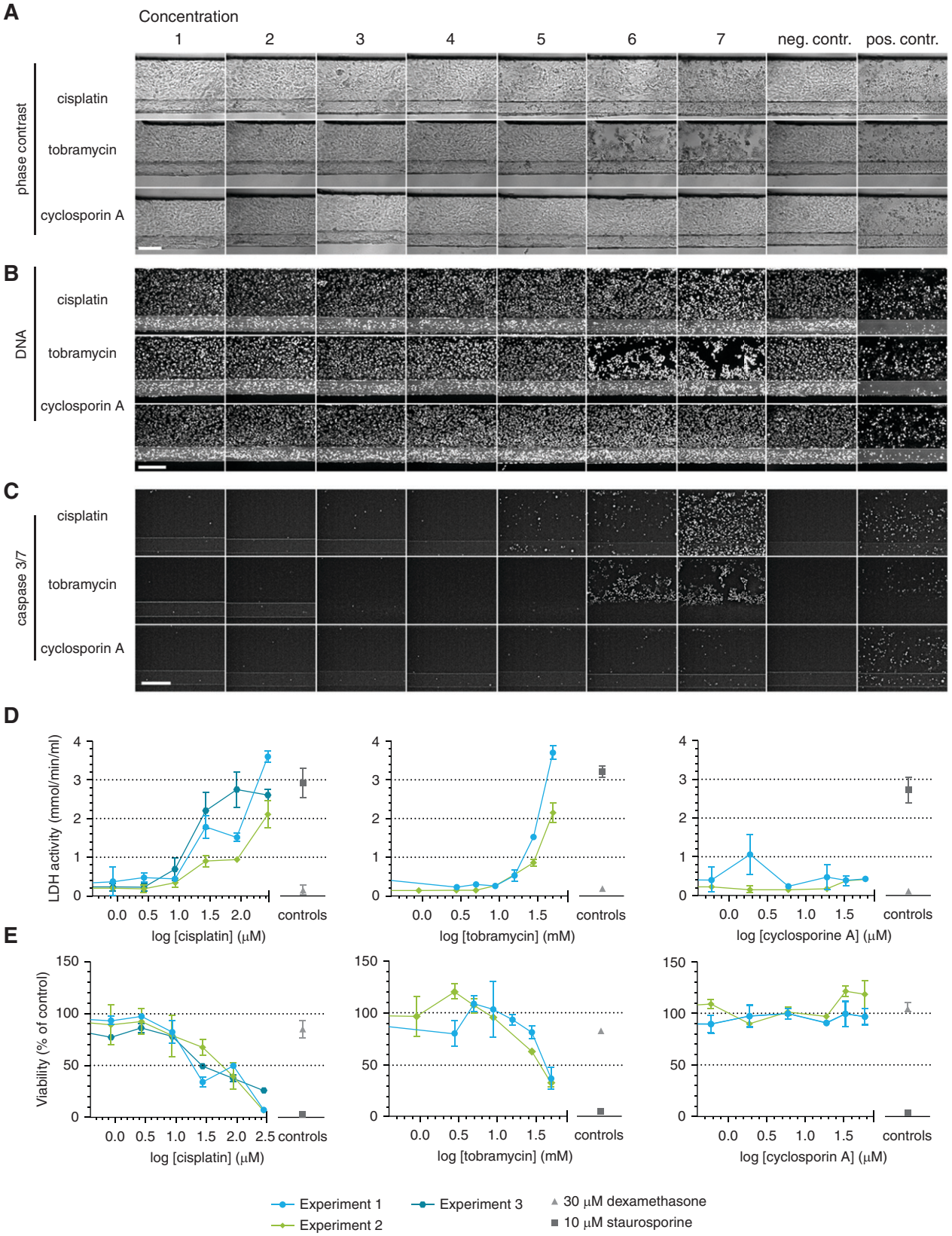

Figure 3. | A panel of assays shows susceptibility of the proximal tubule to AKI in response to nephrotoxic drugs. Cocultures were exposed to concentrations ranges of cisplatin, tobramycin, and cyclosporin A for 48 hours. (A–C) Phase-contrast imaging (A), DNA staining (B), and caspase-3/7 staining (C) showed cell damage after cisplatin and tobramycin exposure in a dose-dependent manner. Representative images. Scale bar, 200 μm. (D) Lactate dehydrogenase (LDH) release in the medium was measured and showed cell damage after cisplatin

to the highest concentration of CysA showed a slight increase in the number of positive caspase-3/7 cells, although this effect was less dominant compared with the other two compounds.

LDH activity released into the medium was measured at the luminal side of RPTEC as an indicator of kidney cell damage (45,46). A trend of dose-dependent increase in LDH release was observed after treatment with cisplatin and tobramycin, whereas such a trend was not observed with CysA (Figure 3D).

Dehydrogenase activity was measured as a representation of cell viability through a WST-8 assay (Figure 3E) (47,48). Cisplatin and tobramycin exhibited a dose-dependent reduction, whereas CysA did not affect the cell viability.

HUVEC were damaged to a similar level as RPTEC when exposed to cisplatin and tobramycin, but more severely after an exposure to CysA (data not shown).

Ischemia Can Be Induced through Nonflow, Low Glucose, and/or Lowering Oxygen Levels

To model rIRI in the proximal tubule-on-a-chip with blood vessel, cultures were exposed to combinations of three different ischemic assaults: low oxygen (5% O_2 incubator, termed "L"), no perfusion (static, termed "S"), and glucose-free and nutrient-poor medium (termed "-glu"; see Table 2 for an overview of ischemic parameter combinations). After a 24-hour exposure, cultures were reperfused under normoxic conditions (21% oxygen, termed "N"; perfusion on the rocker, termed "P"; and glucose- and nutrient-rich medium (5% FBS), termed "+glu," for another 24 hours; Figure 4).

Phase-contrast images of the proximal tubule after 24-hour exposure are shown in Figure 4C. Among the eight different combinations of ischemic parameters, N+S-glu, L+P-glu, and L+S-glu conditions showed rounded-up and clustered morphology. Endothelial vessels showed less severe or no damage under these conditions (Supplemental Figure 1A, top). After the reperfusion, the damage to the proximal tubules had worsened (Figure 4C, bottom). Most parts of the channels of RPTEC exposed to N+S-glu and L+S-glu were washed out during reperfusion, whereas HUVEC stayed attached, even after the washing steps involved in the staining process (Figure 4D and Supplemental Figure 1B, respectively). Caspase-3/7 activity was determined directly after the reperfusion and showed clear activation in RPTEC when exposed to L+S-glu (Figure 4E). A fainter staining was detected in the HUVEC in the same condition (Supplemental Figure 1C). In addition to the L+S-glu condition, caspase-3/7 activation of a few cells was detected in the L+P-glu condition in both cell types, again with a much lower activation in HUVEC.

Figure 4F displays the LDH activity in culture medium from the RPTEC tubule after 24 hours of ischemia (left panel) and subsequent reperfusion (right panel). Overall, the change in LDH activity was limited in comparison to the positive control staurosporine. Under this premise, N+S-glu, L+P-glu, and L+S-glu conditions increased LDH activity, whereas N+P-glu condition decreased LDH activity. After 24-hour reperfusion, N+S+glu- and L+S+glu-treated cultures also displayed increased LDH activity.

Assessment of the dehydrogenase activity as an index of viability showed a significant decrease of 50% in all RPTEC tubules that had been exposed to N+P-glu, N+S-glu, L+P-glu, and L+S-glu. Remarkably, the cultures exposed to the condition N+P-glu also showed a 50% decrease in dehydrogenase activity, which was not reflected in the LDH release. Dehydrogenase activity measured in the HUVEC cultures was reduced by 60% for all conditions exposed to -glu independent from the other parameters (Supplemental Figure 1).

Adenosine Prevented Degradation of Proximal Tubules under Ischemic Conditions

We assessed the protective effect of adenosine, nicotinamide, and NAC in our rIRI model. Cultures were subjected to the two ischemic conditions, L+P-glu and L+S-glu, during 12- or 24-hour exposure, both followed by 24-hour reperfusion.

In phase-contrast imaging, obvious damage of RPTEC was observed in the L+S-glu condition after 12-hour ischemia with 24-hour reperfusion (Figure 5A). More severe damage was observed after 24-hour ischemia with 24-hour reperfusion (Figure 5B). Treatment with 1 mM adenosine retained RPTEC in the channel (Figure 5, A and B, red squares), whereas disrupted RPTEC were observed when treated with 10-mM nicotinamide or 1-mM NAC. The protective effect of adenosine was confirmed by visualization of the DNA (Figure 5, C and D). In addition, coincubation with adenosine limited the increase of caspase-3/7 activity, whereas in the control condition, all remaining RPTEC were caspase-3/7 positive.

LDH activity in the culture medium is shown in Figure 5, G and I. Coincubation with adenosine led to LDH activity reduction in several of the ischemic conditions. Unexpectedly, 10-mM nicotinamide tended to lower LDH activity at any condition, including the control (Figure 5G). We hypothesize that nicotinamide interferes with the LDH assay because nicotinamide is part of the LDH coenzyme nicotinamide-adenine dinucleotide (NAD+) (49) and can bind to the active site of LDH, thereby lowering the LDH activity (50). To test this hypothesis, nicotinamide was coincubated with staurosporine, a potent inducer of apoptosis (Supplemental Figure 2). Staurosporine exhibited renotoxicity as observed through ans increase of LDH release into the culture media and a decrease in cell viability upon treatment. However, cotreatment with nicotinamide only decreased LDH activity in culture media but had no influence on the measured cell viability. This finding suggests that the LDH

Figure 3. | *Continued*. and tobramycin exposure in a dose-dependent manner. (E) Assessment of the viability relative to the corresponding vehicle control using a WST-8 assay showed a dose-dependent decrease in viability after cisplatin and tobramycin exposure. Dexamethasone (30 μM) was included as a negative control; staurosporine (10 μM) was included as a positive control. Error bars represent standard deviation. Experiments 1–3 are independent repeats of the experiment, $n=2$–4 chips per condition.

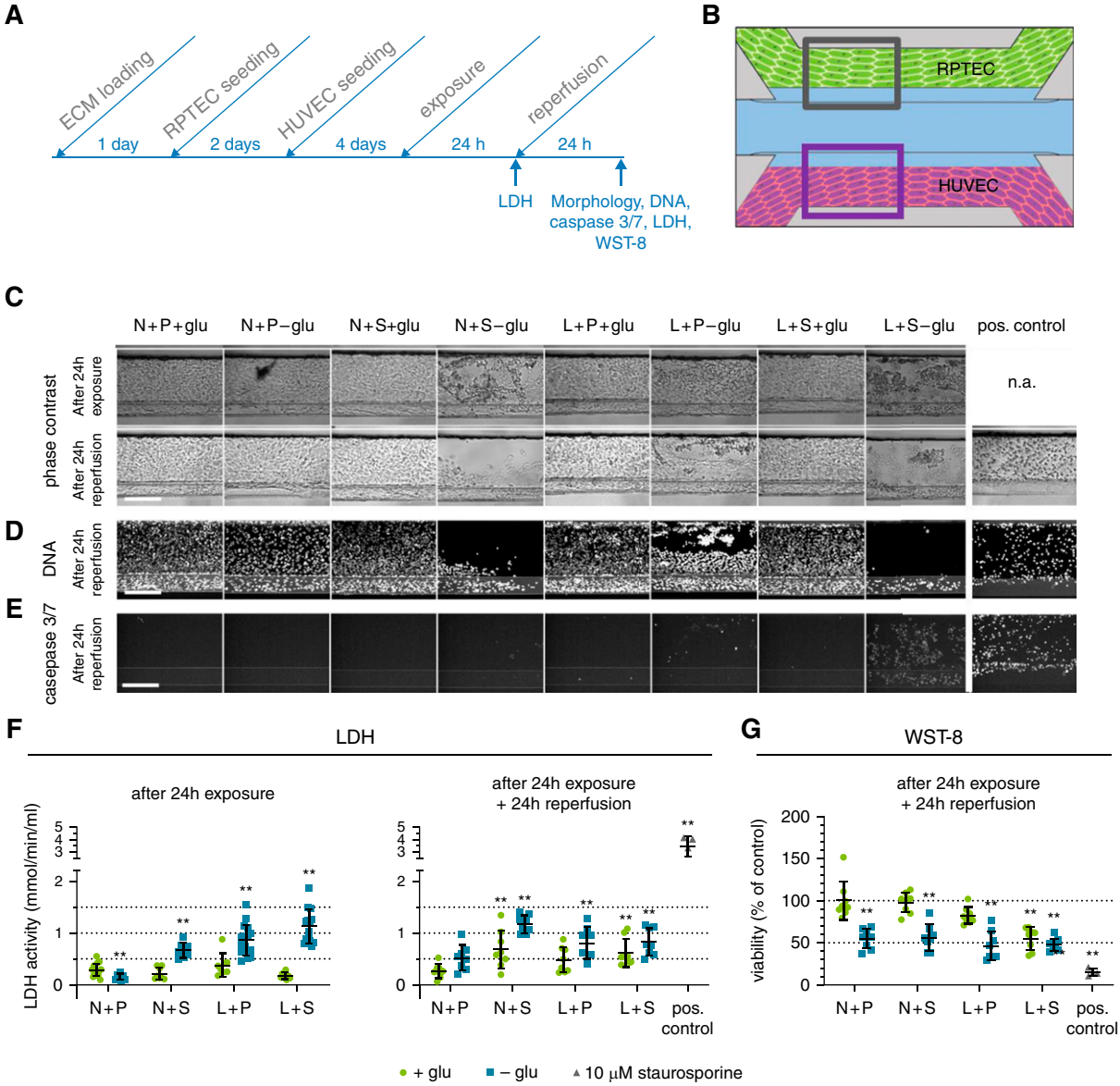

Figure 4. | **Ischemic conditions lead to AKI in the proximal tubule.** Ischemia was modeled on the OrganoPlate coculture through a combination of low oxygen (L), static incubation (S), and glucose- and nutrient-poor medium (-glu) for 24 hours, followed by a 24-hour reperfusion in normoxia (N), perfusion on the rocker (P), and in glucose- and nutrient-rich medium (+glu). (A) Timeline of the experiment. (B) Region of the RPTEC tubule (gray square) that is used for the images shown in (C–E). (C) Representative phase-contrast images after 24-hour exposure (top) and subsequent 24-hour reperfusion (bottom). Different ischemia inducing conditions were tested (columns) and compared with the normal condition N+P+glu. n.a., not available. (D) DNA staining after 24-hour reperfusion. (E) Caspase-3/7 staining after 24-hour reperfusion. Scale bar, 200 μm. (F) LDH release in the medium was measured after 24-hour exposure (left) and 24-hour exposure plus 24-hour reperfusion (right), respectively. (G) WST-8 viability relative to the normal condition N+P+glu was assessed after 24-hour reperfusion. Staurosporine (10 μM) was included as a positive control. Error bars represent standard deviation. One-way ANOVA compares the conditions to the N+P+glu control condition, $^{**}P<0.01$, $n=8$–16 chips per condition.

assay is not suitable for evaluating the renoprotective effect of nicotinamide.

Analysis of the viability by quantifying WST-8 reduction showed a decreased viability upon the ischemic event to approximately 60% of the normoxic control condition after 12-hour exposure to L+S-glu and 35% after the exposure for 24 hours to L+S-glu. No compound appeared to be protective against ischemic damage in the WST-8 assay (Figure 5, H and J). Results of a repetition of the experiments can be found in Supplemental Figure 3. Results indicate the reproducibility of the experiments after both exposure durations, 12 and 24 hours.

Real-Time Caspase-3/7 Imaging Confirms Adenosine Is Protective against rIRI

The activation of caspase-3/7 during the ischemia and reperfusion process was investigated through time-lapse fluorescent microscopy (Figure 6 and Supplemental Video).

While exposed to ischemia (L+S-glu), caspase-3/7 activity increased over time in the medium control and

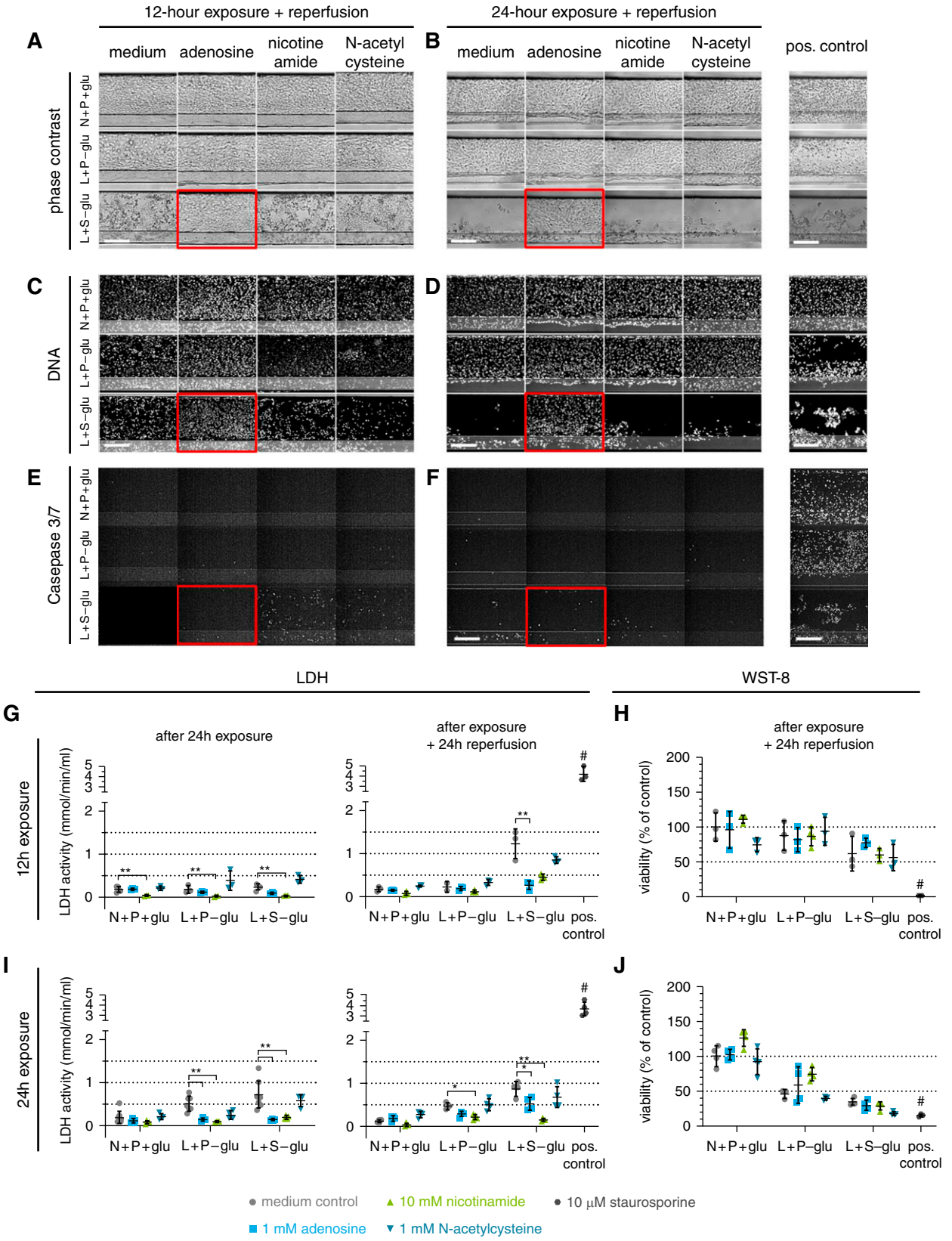

Figure 5. | Coincubation with adenosine decreases ischemia-induced AKI. Cultures were exposed to the selected ischemic conditions L+P-glu and L+S-glu for either 12 or 24 hours, followed by a 24-hour reperfusion, in the presence of adenosine, nicotinamide, or N-acetylcysteine. N+P+glu medium only is the normoxic control condition. (A–F) Images of a region of the RPTEC tubule (see Figure 4B) after 12-hour exposure and reperfusion (A, C, and E) or after 24-hour exposure and reperfusion (B, D, and F). Red squares

adenosine-treated conditions (Figure 6A). Upon reperfusion with fresh medium, severe damage to the RPTEC in the medium control was observed because of cells being washed away (Figure 6B, top-left panel), whereas proximal tubules treated with adenosine remained (Figure 6B, top-right panel). After 12 and 24 hours of the reperfusion process, detached RPTEC and an increase of activated caspase-3/7 in the remaining RPTEC were observed in the medium control, whereas there were no severely disturbed RPTEC observed with adenosine treatment. HUVEC vessels recovered from the ischemic event, independent of adenosine coincubation.

Discussion

In this study, we presented a human renal proximal tubule-on-a-chip in coculture with a perfused blood vessel separated by an ECM with the purpose of modeling rIRI-induced AKI (Figure 1). A 3D reconstruction of histochemical staining's of the cocultures obtained by confocal microscopy showed that RPTEC and HUVEC adhere to the ECM and the side walls in the shape of tubular/vessel structures with lumen formation (Figure 2). Correct polarization of the RPTEC was shown by a staining against the brush border marker ezrin. Primary cilia labeled with acetylated tubulin were observed on the apical surface of RPTEC, and ZO-1, which is a key molecule of tight junctions, was found at the borders of the cells. Consistent with prior work (26), RPTEC formed barriers with limited diffusion of large molecules such as fluorescein-labeled dextran (4.4 and 150 kDa; data not shown), suggesting that the barrier function is well maintained. Although this model is used in the present study, there is room for further modifications. For instance, immune cells could be added to the lumen of the endothelial vessel, allowing the investigation of translocation of immune cells by the endothelium and their role in inflammation of the kidney microenvironment.

To apply this new culture setup to *in vitro* AKI disease modeling, the response of the model to several renotoxicants was tested, and the feasibility of measuring cellular damage was assessed using several assays. Cisplatin, tobramycin, and CysA were capable of affecting RPTEC in the advanced model, as shown in Figure 3. Cisplatin showed a toxic effect in the tested assays, with close resemblance to *in vivo*, as previously reported for this proximal tubule source (51). Tobramycin showed toxicity from 28.1 mM, which is higher than concentrations used clinically (around 2 μg/ml) (52). In clinical settings, the nephrotoxicity of tobramycin is observed after multiple ingestions (52), whereas in the present study, tobramycin exposure was performed at a single dosing for 48 hours. Using a longer time frame with repeated dosing, a toxic effect might be detected at lower concentrations. CysA treatment resulted in increased caspase-3/7 activity at 60 μM. Li *et al.* (53) reported caspase-3/7 activation by CysA with an EC50 of 11 μM in a two-dimensional culture setting of the same cell source (RPTEC SA7K clone). It would be interesting to compare the expression levels of P-glycoprotein, an ABC-transporter, between these culture settings because CysA is a substrate of P-glycoprotein (54). Different levels could potentially cause a change in the intracellular concentration of CysA and that of other toxicants, explaining the differences between different setups. In conclusion, all assays were suitable for detecting reasonable cellular responses, and we decided to use the model for disease modeling of rIRI.

We modeled an ischemic event on the kidney-on-a-chip by exposing the culture to a combination of three ischemic parameters: low oxygen (5%; L), no perfusion (S), and nutrient/glucose-poor medium (-glu), and combinations of the three. After exposure, reperfusion was reinstated under normal conditions (N+P+glu). When exposed to combined culture conditions (summarized in Table 2), N+S-glu, L+P-glu, and L+S-glu were damaged after the 24-hour exposure followed by reperfusion (Figure 4). A significant change was observed in tubular morphology: rounded and detached cells were observed. Moreover, increased caspase-3/7 activity was observed in the remaining epithelial cells after ischemia–reperfusion (L+S-glu or L+P-glu). An incremental increase in loss of viability, as measured by both the release of LDH and enzymatic activity, was observed for the three parameters. Here, we chose to measure kidney cell damage through the release of LDH into the culture media. Zager *et al.* showed LDH is a useful marker for monitoring kidney tubular injury (46). Another biomarker to assess kidney damage would be KIM-1 release (55). Future panel studies will help to select the best biomarker reflecting rIRI. Reduction of the oxygen level in the incubator (L) leads to lower oxygen concentrations in the embedded tissues, which is further reduced by the loss of perfusion flow (S). Loss of flow also reduces the removal of waste products and the availability of nutrients, which is shown to negatively influence the viability by the third manipulated parameter, the nutrient richness of the medium (-glu).

We investigated the potential renoprotective effects of adenosine, nicotinamide, and NAC when cotreated during the rIRI event of the two selected ischemic conditions L+P-glu and L+S-glu. A protective effect of the coincubation with adenosine was observed in the morphology and DNA assessment, caspase-3/7 activation, and LDH release. However, dehydrogenase activity measured with the WST-8 viability assay showed no effect of adenosine. On the basis of these results, we hypothesize that adenosine exerts its protection by lowering the cell metabolism (56), including the dehydrogenase activity. By putting the

Figure 5. | *Continued*. indicate a protective effect of adenosine compared with the medium control of the same ischemic condition in phase-contrast imaging (A and B), DNA staining (C and D), and caspase-3/7 staining (E and F). Scale bar, 200 μm. (G and I) LDH activity and (H and J) WST-8 viability relative to the N+P+glu medium control after exposure to the ischemic condition for 12 hours (G and H) or 24 hours (I and J) followed by reperfusion for 24 hours for both conditions. One-way ANOVA compares the coincubations with the medium control of the same ischemic condition. *$P<0.05$; **$P<0.01$. #, positive control differs significantly with all medium controls ($P<0.01$). Error bars represent the standard deviation. Staurosporine (10 μM) was included as a positive control. $n=3$–8 chips per condition. Both experiments (12- and 24-hour exposure) were repeated (Supplemental Figure 2).

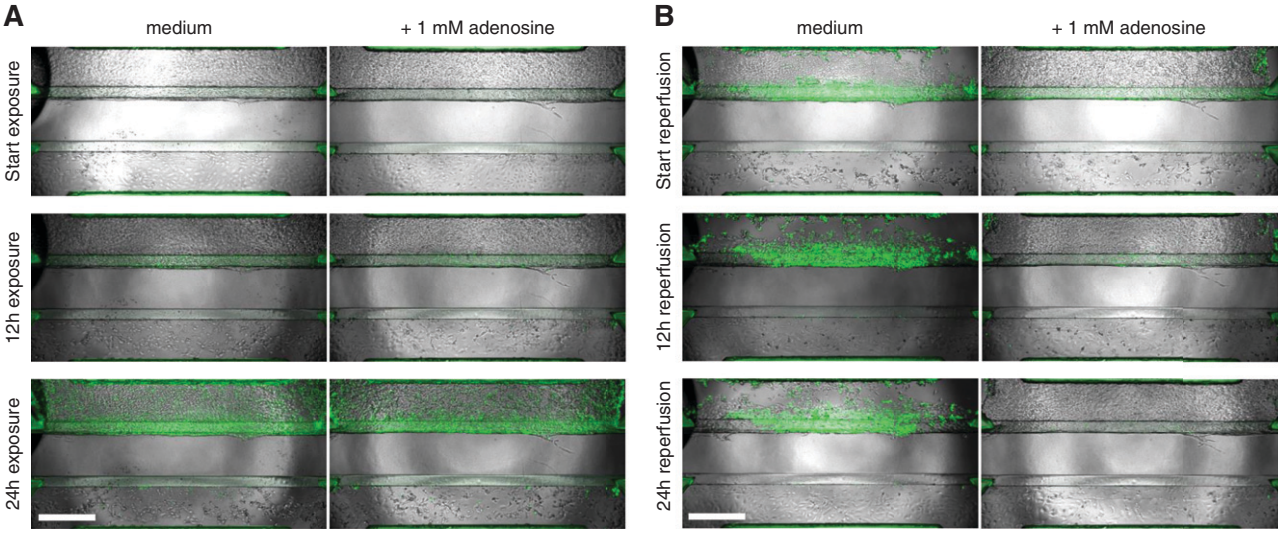

Figure 6. | Real-time caspase-3/7 activation and phase-contrast imaging shows the protective effect of adenosine upon ischemic exposure. (A) Cultures, coincubated with and without 1-mM adenosine, were exposed to ischemic conditions (L+S-glu) for 24 hours, and caspase-3/7 activity was monitored over time. (B) Medium was refreshed to standard culture medium, and cocultures were reperfused under normal conditions (N+P+glu) for 24 hours. Green: activated caspase-3/7. Scale bar: 500 μm. Representative images of $n=3$ chips per condition. A corresponding time-lapse movie can be viewed in the Supplemental Video.

cells in a resting phase with low metabolism, the oxygen demand of the cells is minimal, which could prevent damage from the ischemic condition. Furthermore, adenosine protected against the loss of cells after reperfusion, allowing regrowth of the proximal tubule.

In contrast to adenosine, NAC did not show a renoprotective effect. There are positive reports of NAC being protective in animal rIRI models. The fact that we did not see a protective effect in our human rIRI model could point toward a species-to-species difference, and that NAC does not have a protective effect in humans. In fact, the KDIGO Clinical Practice Guideline for AKI (57) does not recommend using NAC for prevention of postsurgical AKI. We recommend follow-up research to further validate this hypothesis and to support the better understanding of the translatability of this model to humans. In this regard, time-lapse imaging (Figure 6 and Supplemental Video) can be a powerful tool for monitoring the changes of cellular appearance.

Nicotinamide is one of the precursors of nicotinamide adenine dinucleotide (NAD+), lately considered for its therapeutic potential as a NAD booster (58). Recently, results of a phase 1 pilot study administrating nicotinamide was reported (29,59). In patients undergoing cardiac surgery, an increase of precursors for NAD+ was observed in their serum and urine accompanied by a decrease of serum creatinine. In contrast to our expectations, nicotinamide did not prevent tubular damage in our *in vitro* rIRI model. A decrease of LDH activity after nicotinamide treatment contributed to the interference of nicotinamide with the assay, as described in the Results section. Follow-up studies will also help to understand the translatability of this model to humans better. In this regard, time-lapse imaging (Figure 6 and Supplemental Video) can be a powerful tool for monitoring the changes in cellular appearance. We selected a 12- or 24-hour duration for mimicking the ischemic exposure, whereas this duration might be too long to observe the renoprotective effect of nicotinamide. Further assay optimization facilitated by such live imaging should be undertaken to investigate a broader range of various ischemic conditions and treatments at multiple evaluation time points.

Endothelium appeared more tolerant of ischemic injury compared with epithelium, and showed recovery during reperfusion, independent of the treatment condition (Figures 4 and 6 and Supplemental Figure 3). The ability of both endothelial and epithelial vessels to recover during reperfusion upon treatment is an interesting phenotypic assay addition in the search for new protective compounds next to the more traditional readouts on cell death and viability.

In an earlier study, it was shown that glomerular specific endothelium is key to mimic specific aspects of the glomerulus, including glomerular-specific ECM components (60). We therefore expect that the translatability of our model could be further increased by replacing HUVEC with endothelial kidney cells. Alternatively, induced pluripotent stem cell–derived cells could be included to study different genetic backgrounds and predispositions. We also anticipate using of urine-derived tubuloids (61) to capture patient-specific responses to ischemic events.

The current model is sufficiently robust to push forward to a high-throughput phenotypic screen for finding novel protective compounds that protect the kidney during ischemia and reperfusion. The OrganoPlate platform used in this study is compatible, next to general laboratory equipment, with high-content (fluorescent) microscopes and robotics. The 40 chips per plate brings this organ-on-a-chip model to a level of throughput compatible with screening larger compound sets. Kane *et al*. have already reported automation of the system for neuronal cultures (62). Importantly, we showed that we could measure the response to these effects with various orthogonal assays. This allows internal hit verification in a single run.

In conclusion, we successfully expanded our human renal proximal tubule-on-a-chip to a coculture setting with endothelial cells. We were able to study the effect of ischemic conditions and their role in AKI induction by adjusting various culture settings (nutrient composition, oxygen tension, and perfusion flow). We found that ischemic conditions had a strong detrimental effect on the proximal tubule, but only mildly affected the endothelium. We furthermore confirmed that adenosine had a protective effect. We thus conclude that we have established a powerful platform to study AKI *in vitro* that will prove useful to advance our understanding of the pathophysiologic nature of rIRI and support development of novel therapies for preventing AKI.

Disclosures

L. Gijzen, H.L. Lanz, L.M. Tool, R. van Vught, M.K. Vormann, and P. Vulto are employees of MIMETAS BV, The Netherlands, which is marketing the OrganoPlate. T. Hankemeier and P. Vulto are shareholders of that same company. OrganoPlate is a trademark of MIMETAS BV. All remaining authors have nothing to disclose.

Funding

This research project was supported by funding from Astellas Pharma, Inc.

Author Contributions

F. Kiyonaga, H.L. Lanz, M. Ohbuchi, K. Tetsuka, and M.K. Vormann were responsible for the conception and design; L.M. Tool, L. Gijzen, M. Ohbuchi and M.K. Vormann were responsible for the acquisition of the data; A. Fujimori, L. Gijzen, T. Goto, T. Hankemeier, T. Kawabe, F. Kiyonaga, H.L. Lanz, M. Ohbuchi, K. Tetsuka, L.M. Tool, R. van Vught, and M.K. Vormann were responsible for the analysis and interpretation of the data; M.K. Vormann, H.L. Lanz, and K. Tetsuka designed the methodology; M.K. Vormann organised the investigation and the project administration; H.L. Lanz, K. Tetsuka, and P. Vulto provided supervision; H.L. Lanz, K. Tetsuka, M.K. Vormann, and P. Vulto wrote the original draft; and all authors reviewed and edited the manuscript.

Data Sharing Statement

All data are included in the manuscript and/or supporting information.

Supplemental Material

This article contains the following supplemental material online at http://kidney360.asnjournals.org/lookup/suppl/doi:10.34067/KID.0003622021/-/DCSupplemental.

Supplemental Figure 1. Modelling AKI upon ischemic parameter exposure showing results of HUVEC

Supplemental Figure 2. LDH activity and WST-viability measured on cocultures exposed to staurosporine with and without coincubation 33 of nicotinamide (NA)

Supplemental Figure 3. Repetition of experimental data presented in Figure 5 of the main text. Cultures were exposed to the selected 21 ischemic conditions L+P-glu and L+S-glu for either 12 or 24 hours, followed by a 24-hour reperfusion, in the presence of 22 adenosine, nicotinamide or N-acetylcysteine. N+P+glu medium only is the normoxic control condition.

Supplemental Video

References

1. Zuk A, Bonventre JV: Acute kidney injury. *Annu Rev Med* 67: 293–307, 2016 https://doi.org/10.1146/annurev-med-050214-013407
2. Lewington AJP, Cerdá J, Mehta RL: Raising awareness of acute kidney injury: A global perspective of a silent killer. *Kidney Int* 84: 457–467, 2013 https://doi.org/10.1038/ki.2013.153
3. Basile DP, Anderson MD, Sutton TA: Pathophysiology of acute kidney injury. *Compr Physiol* 2: 1303–1353, 2012 https://doi.org/10.1002/cphy.c110041
4. Perazella MA: Renal vulnerability to drug toxicity. *Clin J Am Soc Nephrol* 4: 1275–1283, 2009 https://doi.org/10.2215/CJN.02050309
5. Soltoff SP: ATP and the regulation of renal cell function. *Annu Rev Physiol* 48: 9–31, 1986 https://doi.org/10.1146/annurev.ph.48.030186.000301
6. Hansell P, Welch WJ, Blantz RC, Palm F: Determinants of kidney oxygen consumption and their relationship to tissue oxygen tension in diabetes and hypertension. *Clin Exp Pharmacol Physiol* 40: 123–137, 2013 https://doi.org/10.1111/1440-1681.12034
7. Makris K, Spanou L: Acute kidney injury: Definition, pathophysiology and clinical phenotypes. *Clin Biochem Rev* 37, 85–98, 2016
8. Bonventre JV, Yang L: Cellular pathophysiology of ischemic acute kidney injury. *J Clin Invest* 121: 4210–4221, 2011 https://doi.org/10.1172/JCI45161
9. Malek M, Nematbakhsh M: Renal ischemia/reperfusion injury; From pathophysiology to treatment. *J Renal Inj Prev* 4: 20–27, 2015 https://doi.org/10.12861/jrip.2015.06
10. Kinsey GR, Li L, Okusa MD: Inflammation in acute kidney injury. *Nephron Exp Nephrol* 109: e102–e107, 2008 https://doi.org/10.1159/000142934
11. Nadim MK, Forni LG, Mehta RL, Connor MJ Jr, Liu KD, Ostermann M, Rimmelé T, Zarbock A, Bell S, Bihorac A, Cantaluppi V, Hoste E, Husain-Syed F, Germain MJ, Goldstein SL, Gupta S, Joannidis M, Kashani K, Koyner JL, Legrand M, Lumlertgul N, Mohan S, Pannu N, Peng Z, Perez-Fernandez XL, Pickkers P, Prowle J, Reis T, Srisawat N, Tolwani A, Vijayan A, Villa G, Yang L, Ronco C, Kellum JA: COVID-19-associated acute kidney injury: Consensus report of the 25th Acute Disease Quality Initiative (ADQI) Workgroup [published correction appears in *Nat Rev Nephrol* 16: 765, 2020 10.1038/s41581-020-00372-5]. *Nat Rev Nephrol* 16: 747–764, 2020 https://doi.org/10.1038/s41581-020-00356-5
12. Lieberthal W, Nigam SK: Acute renal failure. II. Experimental models of acute renal failure: imperfect but indispensable. *Am J Physiol Renal Physiol* 278: F1–F12, 2000 https://doi.org/10.1152/ajprenal.2000.278.1.F1
13. Skrypnyk NI, Siskind LJ, Faubel S, de Caestecker MP: Bridging translation for acute kidney injury with better preclinical modeling of human disease. *Am J Physiol Renal Physiol* 310: F972–F984, 2016 https://doi.org/10.1152/ajprenal.00552.2015
14. Russ AL, Haberstroh KM, Rundell AE: Experimental strategies to improve in vitro models of renal ischemia. *Exp Mol Pathol* 83: 143–159, 2007 https://doi.org/10.1016/j.yexmp.2007.03.002
15. van Duinen V, Trietsch SJ, Joore J, Vulto P, Hankemeier T: Microfluidic 3D cell culture: From tools to tissue models. *Curr Opin Biotechnol* 35: 118–126, 2015 https://doi.org/10.1016/j.copbio.2015.05.002
16. Wilmer MJ, Ng CP, Lanz HL, Vulto P, Suter-Dick L, Masereeuw R: Kidney-on-a-chip technology for drug-induced nephrotoxicity screening. *Trends Biotechnol* 34: 156–170, 2016 https://doi.org/10.1016/j.tibtech.2015.11.001
17. Van Norman GA: Limitations of animal studies for predicting toxicity in clinical trials: Is it time to rethink our current approach? *JACC Basic Transl Sci* 4: 845–854, 2019 https://doi.org/10.1016/j.jacbts.2019.10.008
18. Marx U, Akabane T, Andersson TB, Baker E, Beilmann M, Beken S, Brendler-Schwaab S, Cirit M, David R, Dehne EM, Durieux I, Ewart L, Fitzpatrick SC, Frey O, Fuchs F, Griffith LG, Hamilton GA, Hartung T, Hoeng J, Hogberg H, Hughes DJ, Ingber DE, Iskandar A, Kanamori T, Kojima H, Kuehnl J, Leist M, Li B, Loskill P, Mendrick DL, Neumann T, Pallocca G, Rusyn I, Smirnova L, Steger-Hartmann T, Tagle DA, Tonevitsky A, Tsyb S, Trapecar M, Van de Water B, Van den Eijnden-van

Raaij J, Vulto P, Watanabe K, Wolf A, Zhou X, Roth A: Biology-inspired microphysiological systems to advance patient benefit and animal welfare in drug development. *ALTEX* 37: 365–394, 2020 https://doi.org/10.14573/altex.2001241
19. Tetsuka K, Ohbuchi M, Kawabe T, Goto T, Kiyonaga F, Takama K, Yamazaki S, Fujimori A: Reconstituted human organ models as a translational tool for human organ response: Definition, expectations, cases, and strategies for implementation in drug discovery and development. *Biol Pharm Bull* 43: 375–383, 2020 https://doi.org/10.1248/bpb.b19-01070
20. Lloyd SG, Wang P, Zeng H, Chatham JC: Impact of low-flow ischemia on substrate oxidation and glycolysis in the isolated perfused rat heart. *Am J Physiol Heart Circ Physiol* 287: H351–H362, 2004 https://doi.org/10.1152/ajpheart.00983.2003
21. Vedula EM, Charest JL: *Microfabricated Kidney Tissue Models*, 2nd Ed., edited by Bornstein, JT, Tandon V, Tao SL, Charest JL, Amsterdam,,Elsevier, 2019
22. Duan Y, Gotoh N, Yan Q, Du Z, Weinstein AM, Wang T, Weinbaum S: Shear-induced reorganization of renal proximal tubule cell actin cytoskeleton and apical junctional complexes. *Proc Natl Acad Sci U S A* 105: 11418–11423, 2008 https://doi.org/10.1073/pnas.0804954105
23. Raghavan V, Rbaibi Y, Pastor-Soler NM, Carattino MD, Weisz OA: Shear stress-dependent regulation of apical endocytosis in renal proximal tubule cells mediated by primary cilia [published correction appears in *Proc Natl Acad Sci U S A* 113: E1587, 2016 10.1073/pnas.16020411130. *Proc Natl Acad Sci U S A* 111: 8506–8511, 2014 https://doi.org/10.1073/pnas.1402195111
24. Weinbaum S, Duan Y, Satlin LM, Wang T, Weinstein AM: Mechanotransduction in the renal tubule. *Am J Physiol Renal Physiol* 299: F1220–F1236, 2010 https://doi.org/10.1152/ajprenal.00453.2010
25. McDonough AA: Mechanisms of proximal tubule sodium transport regulation that link extracellular fluid volume and blood pressure. *Am J Physiol Regul Integr Comp Physiol* 298: R851–R861, 2010 https://doi.org/10.1152/ajpregu.00002.2010
26. Vormann MK, Gijzen L, Hutter S, Boot L, Nicolas A, van den Heuvel A, Vriend J, Ng CP, Nieskens TTG, van Duinen V, de Wagenaar B, Masereeuw R, Suter-Dick L, Trietsch SJ, Wilmer M, Joore J, Vulto P, Lanz HL: Nephrotoxicity and kidney transport assessment on 3D perfused proximal tubules. *AAPS J* 20: 90, 2018 https://doi.org/10.1208/s12248-018-0248-z
27. Vriend J, Nieskens TTG, Vormann MK, van den Berge BT, van den Heuvel A, Russel FGM, Suter-Dick L, Lanz HL, Vulto P, Masereeuw R, Wilmer MJ: Screening of drug-transporter interactions in a 3D microfluidic renal proximal tubule on a chip. *AAPS J* 20: 87, 2018 https://doi.org/10.1208/s12248-018-0247-0
28. Suter-Dick L, Mauch L, Ramp D, Caj M, Vormann MK, Hutter S, Lanz HL, Vriend J, Masereeuw R, Wilmer MJ: Combining extracellular miRNA determination with microfluidic 3D cell cultures for the assessment of nephrotoxicity: A proof of concept study. *AAPS J* 20: 86, 2018 https://doi.org/10.1208/s12248-018-0245-2
29. Poyan Mehr A, Tran MT, Ralto KM, Leaf DE, Washco V, Messmer J, Lerner A, Kher A, Kim SH, Khoury CC, Herzig SJ, Trovato ME, Simon-Tillaux N, Lynch MR, Thadhani RI, Clish CB, Khabbaz KR, Rhee EP, Waikar SS, Berg AH, Parikh SM: De novo NAD^+ biosynthetic impairment in acute kidney injury in humans. *Nat Med* 24: 1351–1359, 2018 https://doi.org/10.1038/s41591-018-0138-z
30. Seguro AC, Poli de Figueiredo LF, Shimizu MHM: N-acetylcysteine (NAC) protects against acute kidney injury (AKI) following prolonged pneumoperitoneum in the rat. *J Surg Res* 175: 312–315, 2012 https://doi.org/10.1016/j.jss.2011.05.052
31. Shimizu MHM, Danilovic A, Andrade L, Volpini RA, Libório AB, Sanches TR, Seguro AC: N-acetylcysteine protects against renal injury following bilateral ureteral obstruction. *Nephrol Dial Transplant* 23: 3067–3073, 2008 https://doi.org/10.1093/ndt/gfn237
32. DesRochers TM, Suter L, Roth A, Kaplan DL: Bioengineered 3D human kidney tissue, a platform for the determination of nephrotoxicity [published correction appears in *PLoS One* 8, 2013 10.1371/annotation/fb32f1b8-7397-40be-bbf9-b80e67763043]. *PLoS One* 8: e59219, 2013 https://doi.org/10.1371/journal.pone.0059219
33. Lee HT, Emala CW: Protective effects of renal ischemic preconditioning and adenosine pretreatment: Role of A1 and A3 receptors. *Am J Physiol Renal Physiol* 278, 380–387, 2000, https://doi.org/10.1152/ajprenal.2000.278.3.F380
34. Vulto P, Podszun S, Meyer P, Hermann C, Manz A, Urban GA: Phaseguides: A paradigm shift in microfluidic priming and emptying. *Lab Chip* 11: 1596–1602, 2011 https://doi.org/10.1039/c0lc00643b
35. Schindelin J, Arganda-Carreras I, Frise E, Kaynig V, Longair M, Pietzsch T, Preibisch S, Rueden C, Saalfeld S, Schmid B, Tinevez JY, White DJ, Hartenstein V, Eliceiri K, Tomancak P, Cardona A: Fiji: An open-source platform for biological-image analysis. *Nat Methods* 9: 676–682, 2012 https://doi.org/10.1038/nmeth.2019
36. Raju S, Kavimani S, Uma Maheshwara Rao V, Sriramulu Reddy K: Nephrotoxicants and nephrotoxicity testing: An outline of in vitro alternatives. *J Pharm Sci Res* 3: 1110–1116, 2011
37. Belmokhtar CA, Hillion J, Ségal-Bendirdjian E: Staurosporine induces apoptosis through both caspase-dependent and caspase-independent mechanisms. *Oncogene* 20: 3354–3362, 2001 https://doi.org/10.1038/sj.onc.1204436
38. Jacob KA, Leaf DE, Dieleman JM, van Dijk D, Nierich AP, Rosseel PM, van der Maaten JM, Hofland J, Diephuis JC, de Lange F, Boer C, Kluin J, Waikar SS; Dexamethasone for Cardiac Surgery (DECS) Study Group: Intraoperative high-dose dexamethasone and severe AKI after cardiac surgery. *J Am Soc Nephrol* 26: 2947–2951, 2015 https://doi.org/10.1681/ASN.2014080840
39. Stevenson BR, Siliciano JD, Mooseker MS, Goodenough DA: Identification of ZO-1: A high molecular weight polypeptide associated with the tight junction (zonula occludens) in a variety of epithelia. *J Cell Biol* 103: 755–766, 1986 https://doi.org/10.1083/jcb.103.3.755
40. Egorova AD, van der Heiden K, Poelmann RE, Hierck BP: Primary cilia as biomechanical sensors in regulating endothelial function. *Differentiation* 83: S56–S61, 2012 https://doi.org/10.1016/j.diff.2011.11.007
41. Raghavan V, Weisz OA: Flow stimulated endocytosis in the proximal tubule. *Curr Opin Nephrol Hypertens* 24: 359–365, 2015 https://doi.org/10.1097/MNH.0000000000000135
42. Berryman M, Franck Z, Bretscher A: Ezrin is concentrated in the apical microvilli of a wide variety of epithelial cells whereas moesin is found primarily in endothelial cells. *J Cell Sci* 105: 1025–1043, 1993 https://doi.org/10.1242/jcs.105.4.1025
43. Giannotta M, Trani M, Dejana E: VE-cadherin and endothelial adherens junctions: Active guardians of vascular integrity. *Dev Cell* 26: 441–454, 2013 https://doi.org/10.1016/j.devcel.2013.08.020
44. Hanson KM, Finkelstein JN: An accessible and high-throughput strategy of continuously monitoring apoptosis by fluorescent detection of caspase activation. *Anal Biochem* 564–565, 96–101, 2019 https://doi.org/10.1016/j.ab.2018.10.022.
45. Legrand C, Bour JM, Jacob C, Capiaumont J, Martial A, Marc A, Wudtke M, Kretzmer G, Demangel C, Duval D, Hache J: Lactate dehydrogenase (LDH) activity of the number of dead cells in the medium of cultured eukaryotic cells as marker. *J Biotechnol* 25: 231–243, 1992 https://doi.org/10.1016/0168-1656(92)90158-6
46. Zager RA, Johnson ACM, Becker K: Renal cortical lactate dehydrogenase: A useful, accurate, quantitative marker of *in vivo* tubular injury and acute renal failure. *PLoS One* 8: e66776, 2013 https://doi.org/10.1371/journal.pone.0066776
47. Tominaga H, Ishiyama M, Ohseto F, Sasamoto K, Hamamoto T, Suzuki K, Watanabe M: A water-soluble tetrazolium salt useful for colorimetric cell viability assay. *Anal Commun* 36: 47–50, 1999 https://doi.org/10.1039/a809656b
48. Chamchoy K, Pakotiprapha D, Pumirat P, Leartsakulpanich U, Boonyuen U: Application of WST-8 based colorimetric NAD(P)H detection for quantitative dehydrogenase assays. *BMC Biochem* 20: 4, 2019 https://doi.org/10.1186/s12858-019-0108-1

49. McPherson A Jr: Interaction of lactate dehydrogenase with its coenzyme, nicotinamide-adenine dinucleotide. *J Mol Biol* 51: 39–46, 1970 https://doi.org/10.1016/0022-2836(70)90268-8
50. Forlano AJ: Effect of the components parts of nicotinamide adenine dinucleotide (NAD) as inhibitors of lactic dehydrogenase. *J Pharm Sci* 56: 763–765, 1967 https://doi.org/10.1002/jps.2600560626
51. Vormann MK, Vriend J, Lanz HL, Gijzen L, van den Heuvel A, Hutter S, Joore J, Trietsch SJ, Stuut C, Nieskens TTG, Peters JGP, Ramp D, Caj M, Russel FGM, Jacobsen B, Roth A, Lu S, Polli JW, Naidoo AA, Vulto P, Masereeuw R, Wilmer MJ, Suter-Dick L: Implementation of a human renal proximal tubule on a chip for nephrotoxicity and drug interaction studies. *J Pharm Sci* 110: 1601–1614, 2021 https://doi.org/10.1016/j.xphs.2021.01.028
52. Paquette F, Bernier-Jean A, Brunette V, Ammann H, Lavergne V, Pichette V, Troyanov S, Bouchard J: Acute kidney injury and renal recovery with the use of aminoglycosides: A large retrospective study. *Nephron* 131: 153–160, 2015 https://doi.org/10.1159/000440867
53. Li S, Zhao J, Huang R, Steiner T, Bourner M, Mitchell M, Thompson DC, Zhao B, Xia M: Development and application of human renal proximal tubule epithelial cells for assessment of compound toxicity. *Curr Chem Genomics Transl Med* 11: 19–30, 2017 https://doi.org/10.2174/2213988501711010019
54. Saeki T, Ueda K, Tanigawara Y, Hori R, Komano T: Human P-glycoprotein transports cyclosporin A and FK506. *J Biol Chem* 268: 6077–6080, 1993 https://doi.org/10.1016/S0021-9258(18)53221-X
55. Maass C, Sorensen NB, Himmelfarb J, Kelly EJ, Stokes CL, Cirit M: Translational assessment of drug-induced proximal tubule injury using a kidney microphysiological system. *CPT Pharmacometrics Syst Pharmacol* 8: 316–325, 2019 https://doi.org/10.1002/psp4.12400
56. Yap SC, Lee HT: Adenosine and protection from acute kidney injury. *Curr Opin Nephrol Hypertens* 21: 24–32, 2012 https://doi.org/10.1097/MNH.0b013e32834d2ec9
57. Acute Kidney Injury Work Group: KDIGO clinical practice guideline for acute kidney injury. *Kidney Int* 2[Supp]: 1–138, 2012 https://doi.org/10.1038/kisup.2012.1
58. Rajman L, Chwalek K, Sinclair DA: Therapeutic potential of NAD-boosting molecules: The *in vivo* evidence. *Cell Metab* 27: 529–547, 2018 https://doi.org/10.1016/j.cmet.2018.02.011
59. Bulluck H, Hausenloy DJ: Modulating NAD^+ metabolism to prevent acute kidney injury. *Nat Med* 24: 1306–1307, 2018 https://doi.org/10.1038/s41591-018-0181-9
60. Petrosyan A, Cravedi P, Villani V, Angeletti A, Manrique J, Renieri A, De Filippo RE, Perin L, Da Sacco S: A glomerulus-on-a-chip to recapitulate the human glomerular filtration barrier [published correction appears in *Nat Commun* 10: 4791, 2019 10.1038/s41467-019-12177-7]. *Nat Commun* 10: 3656, 2019 https://doi.org/10.1038/s41467-019-11577-z
61. Schutgens F, Rookmaaker MB, Margaritis T, Rios A, Ammerlaan C, Jansen J, Gijzen L, Vormann M, Vonk A, Viveen M, Yengej FY, Derakhshan S, de Winter-de Groot KM, Artegiani B, van Boxtel R, Cuppen E, Hendrickx APA, van den Heuvel-Eibrink MM, Heitzer E, Lanz H, Beekman J, Murk JL, Masereeuw R, Holstege F, Drost J, Verhaar MC, Clevers H: Tubuloids derived from human adult kidney and urine for personalized disease modeling. *Nat Biotechnol* 37: 303–313, 2019 https://doi.org/10.1038/s41587-019-0048-8
62. Kane KIW, Moreno EL, Hachi S, Walter M, Jarazo J, Oliveira MAP, Hankemeier T, Vulto P, Schwamborn JC, Thoma M, Fleming RMT: Automated microfluidic cell culture of stem cell derived dopaminergic neurons. *Sci Rep* 9: 1796, 2019 https://doi.org/10.1038/s41598-018-34828-3

Received: June 1, 2021 **Accepted:** October 29, 2021

See related editorial, "Functional Drug Screening using Kidney Cells On-A-Chip: Advances in Disease Modeling and Development of Biomarkers," on pages 194–198.